GEOLOGICA CARPATHICA, 2024, 75, 4, 227–242 https://doi.org/10.31577/GeolCarp.2024.14

Metamorphism of meta-ultramafic rocks from the Qori metamorphic complex (Neyriz, Iran): Implications for arc-related metamorphism

ABDOLNASER FAZLNIA[1], MIRMOHAMMAD MIRI[2,✉] and ADEL SAKI[2]

[1]Department of Geology, Urmia University, University Blvd, 5756151818 Urmia city, Iran
[2]Department of Geology, Faculty of Earth Science, Shahid Chamran University of Ahvaz, 6135783151 Ahvaz, Golestan Blvd, Ahvaz, Iran

(Manuscript received June 6, 2024; accepted in revised form September 12, 2024; Associate Editor: Dražen Balen)

Abstract: The Qori metamorphic complex (QMC) is a part of the Sanandaj–Sirjan zone (SaSZ) of Iran that formed as a result of Cimmerian orogenic movements during the Toarcian (upper Early Jurassic). The complex consists mainly of meta-basites and marbles with interlayers of meta-psammitic, meta-ultramafic, and meta-pelitic rocks. Peak metamorphic mineral assemblages in meta-basites and meta-pelites comprise mostly garnet+hornblende+plagioclase+quartz±titanite ±biotite and kyanite+garnet+biotite+plagioclase+quartz±staurolite±muscovite, respectively. The equilibrium assemblage olivine+orthopyroxene+clinopyroxene+amphibole+spinel+ilmenite±chromiferrous magnetite in meta-ultramafic rocks formed at the peak metamorphic condition of these rocks. Geothermobarometry calculations and pseudosection modeling obtained 700–800 °C and 6–8 kbar, respectively. The majority of the minerals represent two events of crystallization, especially the spinel grains with flat and convex-concave chemical profiles for their cores and rims. The continental crust of the southern SaSZ underwent two Barrovian-type metamorphic events resulting in its preservation in the QMC meta-ultramafic rocks. The first one, ca. 187 Ma, occurred in association with crustal thickening during the initiation of Neo-Tethys oceanic lithosphere subduction beneath the Central Iran Plate (southeast Eurasia). The second one, ca. 147 Ma, occurred as a result of crustal thickening in the supra-subduction zone. Retrograde metamorphism at the end of the second metamorphism phase, as well as during outcropping towards the surface, resulted in the formation of clinochlore, serpentine, tremolite, talc, and serpentine. The results show that the peak assemblage occurred during the second metamorphic event in the upper amphibolite–lower granulite facies condition.

Keywords: meta-ultramafic rocks, P–T conditions, pseudosection, Qori metamorphic complex, Sanandaj-Sirjan zone

Introduction

The Qori regional metamorphic complex (QMC) is located in northeast Neyriz (Fig. 1a), which is part of the south Zagros orogenic belt. The belt is divided into a set of three (Fig. 1b) parallel NW–SE trending tectonic zones (Berberian & King 1981; Alavi 1994), namely the Zagros Fold-Thrust Belt (ZFTB), the Sanandaj–Sirjan Zone (SaSZ), and the Tertiary–Quaternary Urumieh–Dokhtar magmatic arc (UDMA). The Zagros is the largest mountain belt with the most active collisional orogen associated with the Arabia/Eurasia convergence. It belongs to the Alpine–Himalayan orogenic system that resulted from the closure of the Neo-Tethys Ocean during the Cretaceous and collision during the Eocene–Oligomiocene (e.g, Berberian & King 1981; Alavi 1994). The tectonic history of these zones as a part of the Tethyan region has been summarized previously by many authors (e.g., Berberian & King 1981; Alavi 1994; Omrani et al. 2008; Khadivi et al. 2012; Mouthereau et al. 2012; Mohajjel & Fergusson 2014; Azizi et al. 2015; Jafari et al. 2023).

✉ corresponding author: Mirmohammad Miri
m.miri@scu.ac.ir

The QMC is located in the southern part of the SaSZ (Fig. 1b). The zone juxtaposes various metamorphic and magmatic rocks that had mainly formed in the Mesozoic. During the Paleozoic, the SaSZ had been part of the northeast Gondwanaland, which was separated from the Eurasian plate by the Paleotethys Ocean (Golonka 2004; Mouthereau et al. 2012; Fazlnia & Alizade 2013; Shafaii Moghadam et al. 2014; Fergusson et al. 2016; Fazlnia 2017a, 2019; Jafari et al. 2023). From the Early Permian to the Early Triassic, the SaSZ was situated along the southern margin of the Eurasian plate, separated from the northern Gondwanaland by the Neo-Tethys Ocean (e.g, Mouthereau et al. 2012; Fergusson et al. 2016; Gharibnejad et al. 2023; Jafari et al. 2023). During the Mesozoic, the Neo-Tethys lithosphere was subducted beneath the Eurasian plate (Golonka 2004; Molinaro et al. 2005; Fazlnia et al. 2009, 2013; Agard et al. 2011; Fergusson et al. 2016; Hassanzadeh & Wernicke 2016; Fazlnia 2017b; Jafari et al. 2015, 2018), and the SaSZ occupied the position of an Andean-type metamorphic–magmatic arc (Berberian & Berberian 1981; Agard et al. 2005, 2011; Mouthereau et al. 2012; Fazlnia et al. 2013; Sepahi et al. 2014; Moinvaziri et al. 2015; Hassanzadeh & Wernicke 2016; Shafaii Moghadam et al. 2016; Shabanian et al. 2018; Fazlnia 2018; Miri & Sepahi 2023). The study of the petrogenesis of the Jurassic granitoids

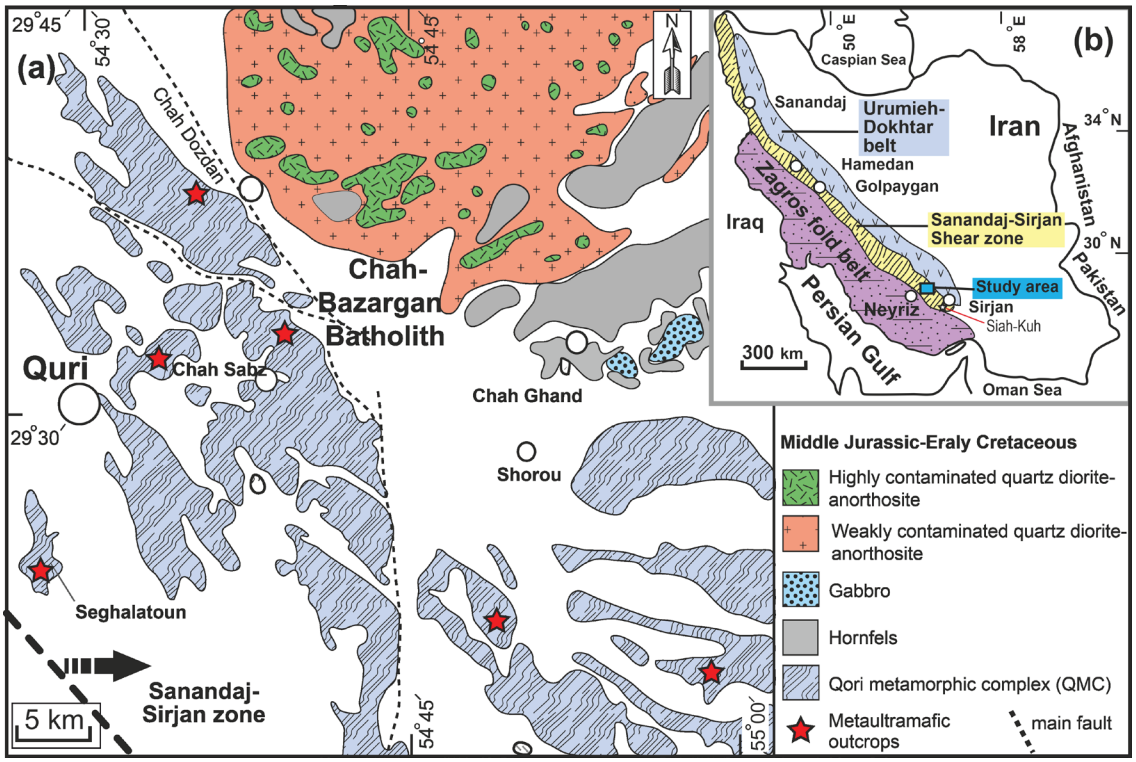

Fig. 1. a — Simplified geological map of northeastern Neyriz and the study area location (modified after Sabzehei et al. 1992). **b** — The inset shows the main tectonic units of Iran (modified after Stöcklin 1968).

(S-type, I-type, and A-type) of the SaSZ (Karimpour et al. 2022) demonstrated that this zone coincided with a subduction system during the Jurassic. In contrast to the subduction model, Azizi & Stern (2019) showed that the central part of the SaSZ during the Jurassic was formed as a result of a continental rift, based on the determination of the genesis and geochemistry of gabbroic to granitic rocks. In addition, Nouri et al. (2023) attributed the magmatic rocks of the central SaSZ to the formation of the transitional crust of a passive continental margin between the Neo-Tethys and Iran continental crust during the Jurassic period. Other works considered a plume-influenced intracontinental rifting model for the Middle Jurassic magmatism of the SaSZ (e.g., Lucci et al. 2023).

The final closure of the Neo-Tethys and the collision of the Arabian and Eurasian plates took place during the Tertiary (Berberian & Berberian 1981; Alavi 1994; Golonka 2004; Molinaro et al. 2005; Omrani et al. 2008; Dilek et al. 2010; Agard et al. 2011; Eyuboglu et al. 2012; Mouthereau et al. 2012; Neill et al. 2013, 2015; Azizi et al. 2015; Jafari et al. 2015; Fazlnia 2018, 2019). Azizi et al. (2015) also found some local collisions in western Iran (some parts of the SaSZ and Central Iran) before the collision of the Arabian and Iranian plates in the Miocene. During the same period, the Zagros Fold-Thrust Belt (ZFTB) was formed as part of the Alpine–Himalayan Mountain chain, extending about 2000 km from eastern Turkey to the Oman line in southern Iran (Berberian & King 1981; Alavi 1994; Agard et al. 2005, 2011; Omrani et al. 2008; Mouthereau et al. 2012).

The QMC in the southern part of the SaSZ evolved during the Jurassic (Fazlnia et al. 2009; Sheikholeslami 2015; Fazlnia 2017b) in association with the Neo-Tethys subduction beneath the Central Iran Plate (CIP; Fazlnia et al. 2009). The present study investigates P–T conditions and petrogenesis of meta-ultramafic rocks from the QMC (Fig. 1) to reconstruct the condition of Neo-Tethys subduction-related metamorphism in the region. The metamorphism occurred at the initiation of subduction and continued throughout the Jurassic (Fazlnia et al. 2009; Gharibnejad et al. 2023). The complexities of lithology around Qori with the function of the fault system have led to drastic changes in the order and sequence of rock outcrops from the Jurassic to the late Cenozoic. Establishing a connection between the Qori Barrovian-type metamorphic complex and Neotethys subduction or rifting can help us understand the tectonic evolution of the southern part of the SaSZ, as well as determine the connection between the southern and northern parts of this zone.

Geological setting

General geological situation

The Qori Barrovian-type metamorphic complex consists of meta-basites (actinolite schist to garnet amphibolite) and marbles, together with interspersed meta-psammitic, meta-ultramafic (olivine–orthopyroxene–clinopyroxene–spinel–

hornblende schist), and meta-pelitic (biotite to garnet–kyanite–biotite schist) layers that underwent medium- to high-grade metamorphism (Fazlnia et al. 2009). Many of the rocks that had formed from the Devonian to the Late Permian were affected by the regional metamorphic event in the Early Jurassic (Sabzehei et al. 1992; Sheikholeslami et al. 2008). The parental rocks of these metamorphic outcrops likely included shale, marble, basalt, granite, and ultramafic rocks. Due to different stages of prograde and retrograde metamorphism, including some lithological variations, such as alteration, weathering, faulting, and tectonic disturbance, it is impossible to identify the primary parental rock of the Qori complex. Therefore, it is difficult to comment on the origin of meta-ultramafic rocks (Fig. 2a, b). In general, the low-grade and high-grade metamorphic rocks crop out in the southwest and northeast of the area, respectively.

Regional metamorphic mineral assemblages in meta-pelites comprise mainly Ky+St+Grt+Bt+Ms+Pl+Qz and Ky+Grt+Bt+Pl+Qz±Ms [the mineral abbreviations (Whitney & Evans 2010) are represented in the Supplementary Table S5]. No evidence of partial melting to produce granitic liquids was found in such metamorphic outcrops. Some sedimentary and low-grade meta-sedimentary rocks crop out among the high-grade metamorphic rocks due to the late-stage shearing of the Zagros fold belt (Berberian & King 1981; Sabzehei et al. 1992; Karimi et al. 2012; Nadimi 2015; Fazlnia 2017b; Honarmand et al. 2017; Mahmoudi & Baharifar 2018; Saki et al. 2020; Lucci et al. 2021). All rock types are strongly sheared and thrust as imbricate slices over the Neyriz ophiolite (Berberian & King 1981; Sheikholeslami et al. 2008; Fazlnia et al. 2009; Sheikholeslami 2015). Fazlnia et al. (2007) estimated 9.2±1.2 kbar and 705±40 °C as peak metamorphic conditions for meta-pelites in the QMC (Chah–Sabz and Seghalaton areas) resulting from crustal thickening during the Early Cimmerian orogeny between 187 and 180 Ma. This event occurred in association with the initiation of the Neo-Tethys subduction beneath Central Iran (Fazlnia et al. 2013). It caused the first crystallization process (M1) in the metamorphic rocks of the area. Like the Qori complex, the Jurassic Shahrekord eclogites from the central SaSZ formed as a result of Neotethys lithosphere subduction beneath Central Iran (Davoudian et al. 2016).

Several million years later, Chah–Bazargan minor gabbroic intrusions intruded the QMC during the subduction at 170.5±1.9 Ma (Fazlnia et al. 2013; Yang et al. 2018). Geochemical and tectonic studies of these gabbros (Yang et al.

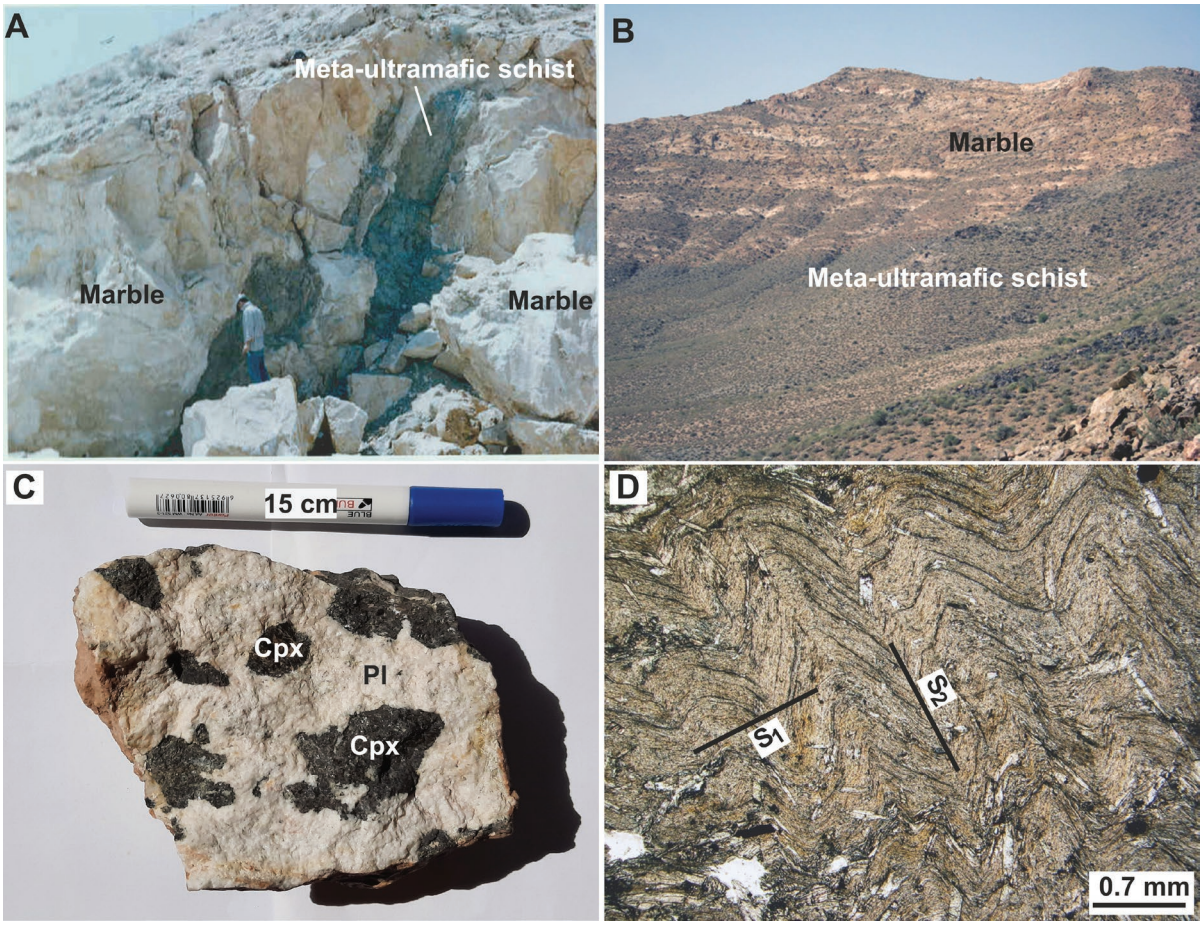

Fig. 2. Field and microscopic photographs from ultramafic schists. **a, b** — Outcrop of ultramafic schists; **c** — Pegmatitic gabbro from the Qori complex; **d** — Plane-polarised transmitted-light photomicrograph showing two kinds of foliations in low-grade parts, S1 and S2.

2018) demonstrated that these rocks formed in a typical continental arc. They concluded that the arc caused Barrovian-type metamorphic events during the Jurassic and stated that the accumulation of mafic melts under the base of the continental crust provided the necessary thermal flow for this metamorphism. Additionally, the west edge of the QMC underwent some Barrovian-type metamorphism at 147 Ma as a result of crustal thickening and the rise of the temperature during the dehydration in the young and hot Neo-Tethys subducted slab in the region (Fazlnia et al. 2009; Fazlnia 2017b). This process was the second phase of metamorphism (M2) in the rocks and caused foliation in the garnet amphibolites. Fazlnia et al. (2009) estimated 7.5 to 9.5 kbar (at a depth of 25 to 32 km) and 680 to 720 °C, based on the Grt–Hbl and Hbl–Pl geothermometers and a Grt–Hbl–Pl–Qz geobarometer for peak P–T condition of M2. A few small pegmatitic gabbro bodies (different from the 170 Ma gabbro bodies; Fig. 2c) cut these rocks showing active magmatism during and after the M2.

Parental rock of the ultramafic schists from the QMC occurs as intercalations in the marbles and amphibolites (Fig. 2a–c). In high-grade metamorphic parts, garnet-amphibolites and olivine–diopside–spinel–scapolite marbles accompany the ultramafic schists, and the presence of low-grade metamorphosed pillow lavas thereby suggests that they had formed in an oceanic environment. Some outcrops also occur near the kyanite–garnet schists.

Petrography

There are two foliations in low-grade meta-ultramafic rocks from the QMC, S1 and S2 (Fig. 2d). The S2 crenulation cleavage is the deformed S_1. The high-grade samples show only the S_2 (Fig. 3a, b), which had developed during the second deformational phase, D_2. The rocks are composed mainly of well-foliated idioblastic Amp together with Ol, Opx, Cpx, Spl, Ilm±Cln±Tlc±Brc±Mag±Stp (Supplementary Table S1 and Fig. 3).

The amphiboles are mostly tremolite in the upper greenschist to low-grade amphibolite facies (Fig. 3a), and magnesio-Hbl in the middle amphibolite facies (Fig. 3b–d). They are in equilibrium with Cln in the upper greenschist to lower amphibolite facies and with spinel in high-grade amphibolite facies. The Ol grains occur as xenoblastic, 1–10 mm long elongated crystals (Fig. 3c). They formed in the high-grade amphibolite facies rocks and are elongated parallel to the main foliation (S_2) in the prograde mineral assemblages of Spl+Ol +Opx+Cpx+Hbl (Fig. 3c, d). Opx and Cpx grains occur only in high-grade amphibolite facies as subidioblastic to idioblastic, 1 to 3-mm elongated crystals. Orientation and elongation of the Ol, Opx, and Cpx indicate they formed during metamorphism and deformation (e.g., Peltonen 1990).

Spl occurs as dark-colored xenoblastic crystals in low-grade rocks, but green and subidioblastic in the amphibolite facies rocks (Fig. 3d). It is darker than Mag and Ilm in BSE images (Fig. 4a–d). The occurrence of Spl, Hbl, Opx, Cpx, and Ol without Chl (Fig. 3b–d) by increasing temperature, suggests metamorphism in the upper amphibolite facies for these rocks. The modal percentage of Ilm is enhanced by increasing the metamorphic grade. In low-grade amphibolites, Spl and Ilm are in equilibrium with Mag (Fig. 4d). Spl replaces Mag and Ilm in the higher metamorphic grades. Cln+Atg+Tr+Tlc+Brc+Qz represent the retrograde mineral assemblage formed after M2, which may be called the M3 metamorphic growth stage, and are either parallel or oblique to the main foliation (Figs. 3b, c, 4a). Cln occurs as 1 to 7 mm idioblastic crystals with polysynthetic twinning that the green Spl replaces in the middle amphibolite facies. Tr formed in the Hbl margins during retrograde metamorphism. Fine-grain Atg, Tlc, and Brc were formed by the hydration of the Ol and Opx (Fig. 3c). High-grade mineral assemblages formed simultaneously with the deformation and are associated with the second phase of the regional Barrovian metamorphism (M_2; Fazlnia et al. 2009).

Research methods

Analytical methods

The chemical compositions of 4 representative samples from the meta-ultramafic rocks were analyzed by XRF (X-ray fluorescence) instrument using a Philips PW 1480. Major elements were measured using fusion beads. The sample LOI (loss on ignition) was determined by heating the sample powders at 1000 °C for 2 hours, and the decrement of powders weights was then calculated. The chemical compositions of the minerals were analyzed using a JEOL JXA-8900 electron probe micro-analyzer (EPMA) system with 15 kV accelerating voltage, a 20 nA probe current, and a 2 µm beam diameter at the University of Kiel, Germany. Counting time on peaks was set to 10–30 s and 5–15 s on backgrounds, respectively, according to the volatility of the element in the beam spot. The following X-ray lines and natural calibration materials (the majority of them are from the Smithsonian Natural Museum of Natural History microbeam references) were used: wollastonite (Si–*Kα*), omphacite (Al–*Kα*), fluorapatite (F–*Kα*; P–*Kα*; Ca–*Kα*), albite (Na–*Kα*), fayalite (Fe–*Kα*; Mn–*Kα*), orthoclase (K–*Kα*), periclase (Mg–*Kα*) and rutile (Ti–*Kα*). The raw data were corrected using the CITZAF method (Armstrong 1995).

Geothermobarometry formulas

Distribution of $Fe^{2+}$and Mg between the coexisting Opx and Ilm has been calibrated as a geothermometer (Anderson et al. 1972; Bishop 1980; Sack & Ghiorso 1991). Ilm is a solid solution between Ilm, $FeTiO_3$, and Gk, $MgTiO_3$. Bishop (1980), based on the exchange of Fe^{2+} and Mg between the coexisting Opx and Ilm, presented the following equation:

$$T(°C)=\frac{1646+1634(Fe^{2+}/(Fe^{2+}+Mg))^{Ilm}+0.0124P}{Ln_{K_D}}-273$$

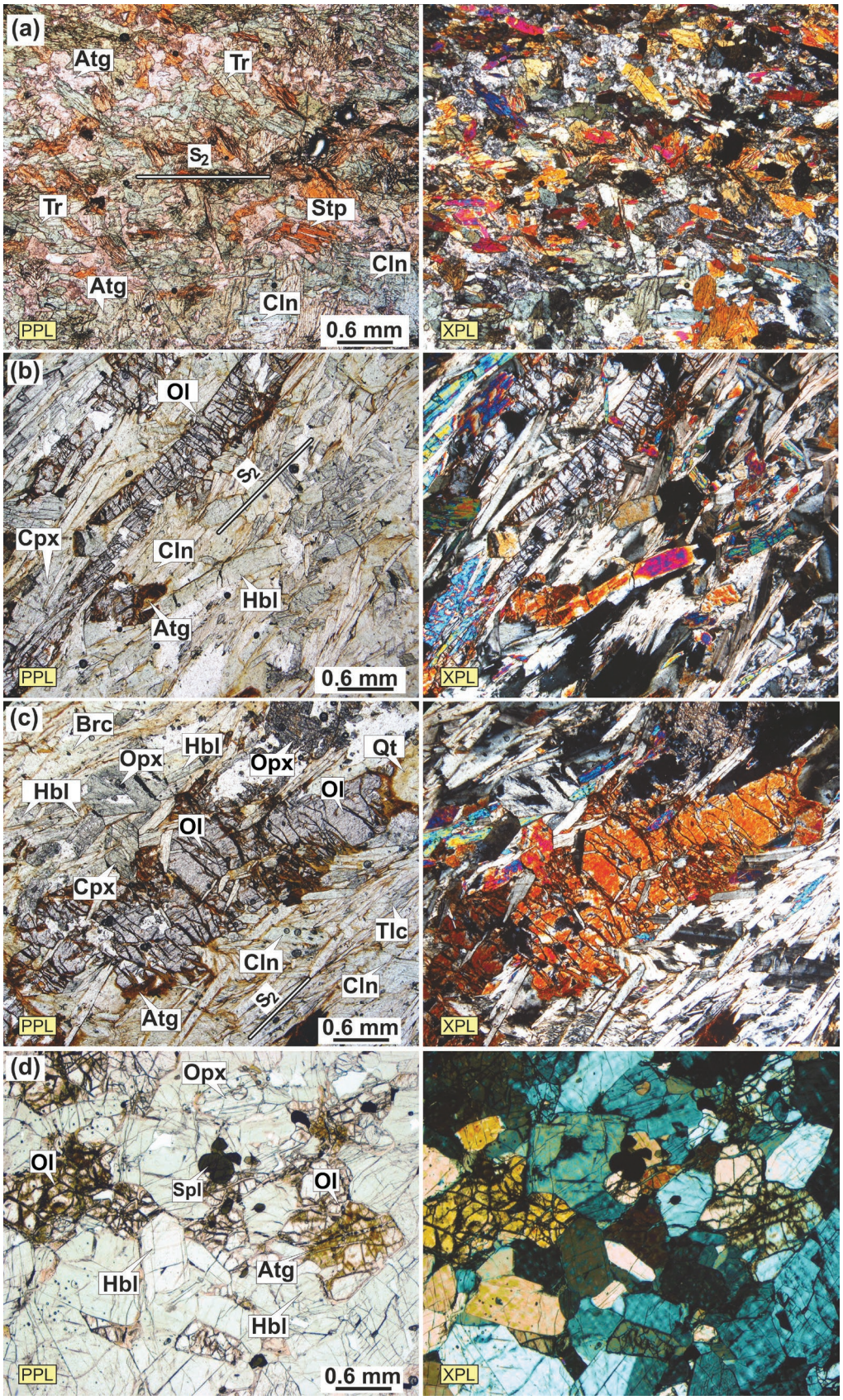

Fig. 3. Series of plane-porlarised (left images) and cross-polarised (right images) transmitted light photomicrographs of ultramafic schists from the QMC. **a, b** — An equilibrium mineral assemblage from low-grade and medium-grade rocks; **c, d** — The equilibrium mineral assemblages from high-grade rocks. Mineral abbreviations from Whitney & Evans (2010).

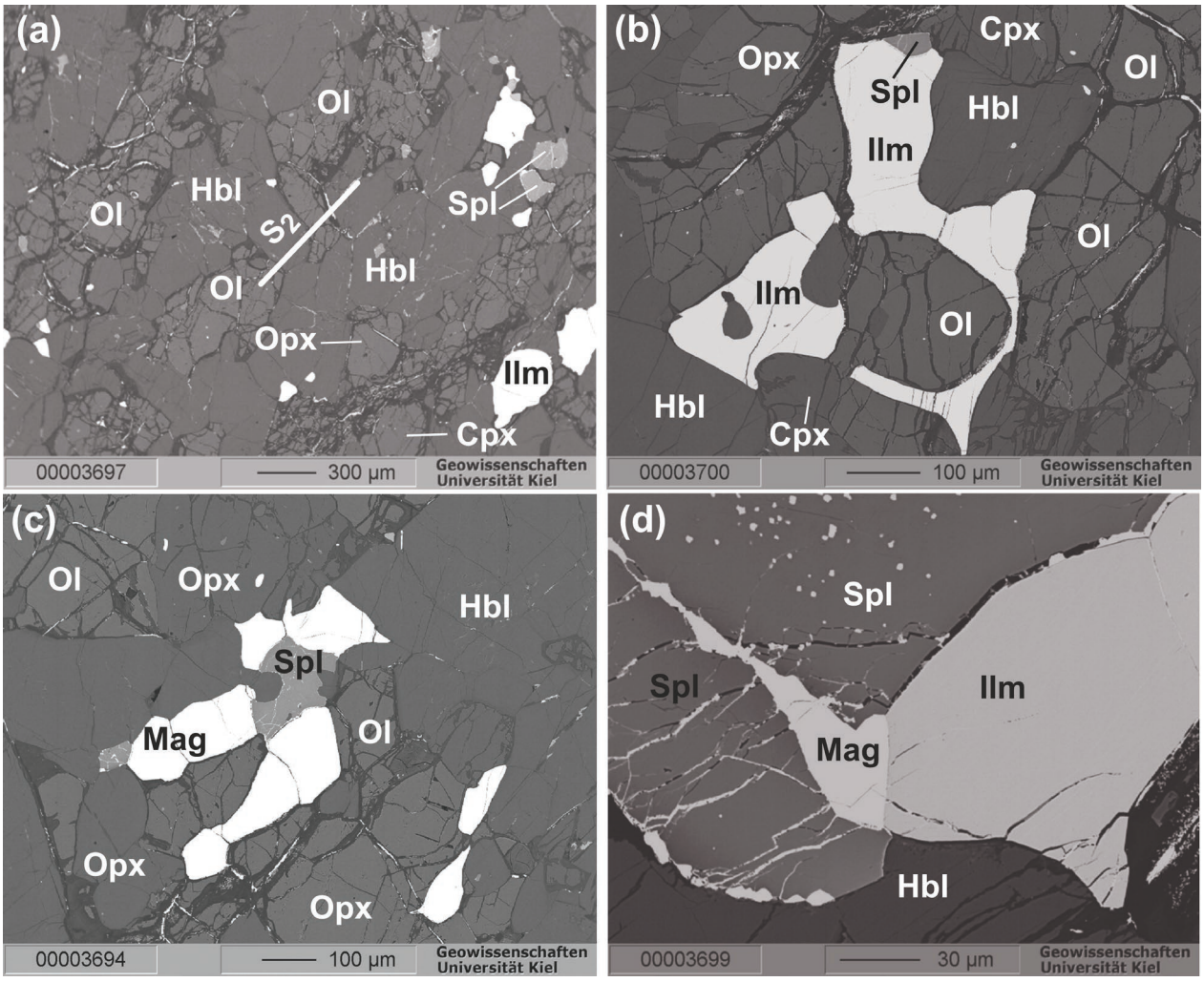

Fig. 4. BSE images of ultramafic schists from the QMC. **a, b** — High-grade metamorphic rocks (samples 55 and 60). Weak S2 foliation in high-grade rocks is present in figure a. **c** — An Equilibrium mineral assemblage from medium- to high-grade rocks. **d** — Textural equilibria between oxide minerals of ilmenite, magnetite, and spinel [see Fusheng et al. (2018) for more discussions of BSE images]. Abbreviations for minerals are shown in Figure 3.

where $K_D=(MgO/FeO)^{Opx}/(MgO/FeO)^{Ilm}$, and P is in bars. The uncertainty (1σ) is ±30 °C.

The other thermometer applied to the studied meta-ultramafic rocks is the experimental calibration of the Al content in Opx in the presence of Ol and Fe–Mg oxide (Gasparik 1985, 1987). It has been shown that the Al content in Opx depends on temperature, pressure, and Al-rich phases, such as Spl (Gasparik 1985, 1987). Al content in the M1 site of Opx is dependent on temperature (Gasparik 1987). Gasparik (1987), based on the Al content in the M1 site of Opx, proposed the following experimental equation:

$$T(\pm 20\,^{\circ}C)=\frac{4011X_{Al}}{1-1.04X_{Al}+\frac{1}{3}Fe/(Fe+Mg)}+443+P(kbar)$$

where X_{Al} is the molar aluminum in the M1 site of Opx and Fe/(Fe+Mg) is the ferrous iron ratio in Opx.

The content of Ca in Opx in the CMS ($CaO–MgO–SiO_2$) system depends on temperature and pressure. The temperature in this system may be calculated from the Ca content of Opx alone (Brey & Köhler 1990):

$$T(\pm 26\,^{\circ}C)=\frac{6425+26.4P}{-LnCa^{Opx}+1.843}$$

Uncertainty (1σ) is ±26 °C for the $CaO–MgO–SiO_2$ (CMS) system and ±20 °C for the natural system experiments.

Calculation of the pseudosection diagram

A phase diagram in NCFMASHTO chemical system ($Na_2O–CaO–FeO–MgO–Al_2O_3–SiO_2–TiO_2–H_2O–O2$) was calculated for the composition of the sample Af55 (Supplementary Table S4) containing the peak metamorphic assemblage olivine+orthopyroxene+clinopyroxene+amphibole+spinel (see

Fig. 8a) using the software Perple_X v. 7.1 (Connolly 2005; downloaded April 14, 2024; https://www.perplex.ethz.ch) and thermodynamic database hp62ver.dat (Holland & Powell 2011) reference dataset. The following solid solution models were used: Chl(W) for Chl, Gt(W) for Grt, Opx(W) for Opx (White et al. 2014), cAmph(G) for Amp, Augite(G) for Cpx, melt(G) for melt (Green et al. 2016), O(HP) for Ol (Holland & Powell 1998), Fsp(C1) for Pl (Holland & Powel 2003), Ilm(WPH) for Ilm (White et al. 2000), and Sp(WPC) for Sp (White et al. 2002). The analyzed LOI was considered a pure H_2O unsaturated fluid with the uppermost (lithospheric) mantle peridotites containing ~4000 ppm H_2O (Green 2015).

Results

Mineral chemistry

Spinel and related minerals

Spl in Tr–Cln–Ol serpentinites (schists) is extremely Al-poor Mag or Cr-Mag (Supplementary Table S2). Cr/Fe^{3+} ratios tend to vary from grain to grain and sometimes within a grain. Alumina contents are meager (approximately 1 % Al–Spl end member).

Mag, Cr-Mag, ferrite-Chr, low Al-Chr, high Al-Chr, and finally Mg–Al-Spl form a continuous series that is, to a large extent, dependent on the metamorphic grade in ultramafic rocks (Evans & Frost 1975). In the middle of the upper amphibolite facies samples (samples 55 and 60, Fig. 5), the green-(Mg–Fe) Al_2O_4-Spl appears to correspond to crystallization simultaneously with enstatite crystallization. Rim-to-rim chemical profiles provided for these Spl grains give various results. In some Spl grains (sample 55), the distribution patterns of Fe, Mg, Cr, Al, and Ti are uniform throughout the crystals (Fig. 5a, c), suggesting the homogenization of the core and rim during the peak of metamorphism. However, some large Spl grains show continuous zoning with high-Cr cores and high-Al, low-Cr, and -Fe rims (sample 60, Fig. 5b, d). In addition, Al and Mg content increases, and Cr and Fe decrease towards the rim of the Spl grains.

The most ubiquitous oxide minerals are Mag, titaniferous Mag, and Ilm. Ilm is present in the matrix and also as the inclusion in other minerals, such as Amp and Opx grains, in the upper greenschist (samples 46 and 42), as well as the lower (sample 69) and middle (samples 55, 56, and 60) amphibolite facies. The modal % of Ilm increases when raising the metamorphic grade. There were no systematic compositional variations from the core to the rim of the inclusion and the matrix Ilm. Ilm from the mineral assemblage of Ol+Amp+Cr-Mag+Ilm+Cln (sample 69) had a higher Hem component than those from the mineral assemblage of Ol+Opx+Cpx+Hbl+Spl+Ilm. This compositional variation could be attributed to the change in the P–T condition in different metamorphic facies.

There were no large and idioblastic grains of Mag in any of the high-grade samples. They occur as accessory phases around Ilm and Spl or as veinlets in Spl (Fig. 4). It is possible that some Mag grains were trapped within Spl and Ilm minerals as a result of the metamorphic prograde reaction. These reactions decreased the modal percentage of Mag and increased the modal percentage of Spl and Ilm. The mutual contact and equilibrium texture for Mag and Ilm most likely exhibited the Ilm–Mag buffer for oxygen fugacity during metamorphism.

Amphibole

The chemical compositions of the Amp grains are represented in Supplementary Table S2. The structural formula was calculated based on 23 oxygen and normalized to 13 cations, except for Ca, Na, and K (13eCNK). The matrix Amp is magnesio-Hbl in the mineral assemblage Ol+Opx+Cpx+Amp+Spl+Ilm (samples 55 and 60), and Tr in the mineral assemblage Ol+Amp+Cr-Mag+Ilm+Cln (samples 46 and 69), according to the nomenclature of Hawthorne et al. (2012) (Fig. 6a). The chemical profiles of the hornblende show that the cores contain higher Si and Mg, but lower Al, Na, and K than the rims, thereby suggesting Amp growth during prograde metamorphism. Moreover, the matrix Tr around the Hbl indicates some retrograde metamorphism.

Olivine, orthopyroxene and clinopyroxene

There were no systematic compositional variations from the core to the rim within single Ol crystals (samples 55 and 60, Supplementary Table S2), even though the core has higher Si and Fe and lower Mg and Ni than the rims, which suggests formation by increasing the metamorphic grade. In comparison with Ol from the higher-grade rocks (samples 55 and 60, middle to upper amphibolite facies), those from the lower-grade rocks (sample 69, lower amphibolite facies) have lower SiO_2, MgO, and NiO and higher FeO and MnO contents.

Opx and Cpx occur only in the samples from the middle and upper amphibolite facies (samples 55 and 60). There are no significant compositional differences between the analyzed crystals. They all plot in the field of enstatite in the pyroxene group ternary classification diagram (Fig. 6b). The chemical profile shows that the cores of the sample 60 Opx have higher Al, but lower Si than the rims, which can be attributed to the formation of the rims during retrograde metamorphism.

Serpentine and clinochlore

Srp and Cln minerals with a platy and fibrous habit are common in the studied samples. They occur as platy crystals (30–50 and 20–40 modal percent, respectively) in the low-grade samples. Srp in high-grade rocks that surround other minerals, such as Ol and Opx, formed due to retrograde reactions during exhumation. All the analyses from the Srp grains

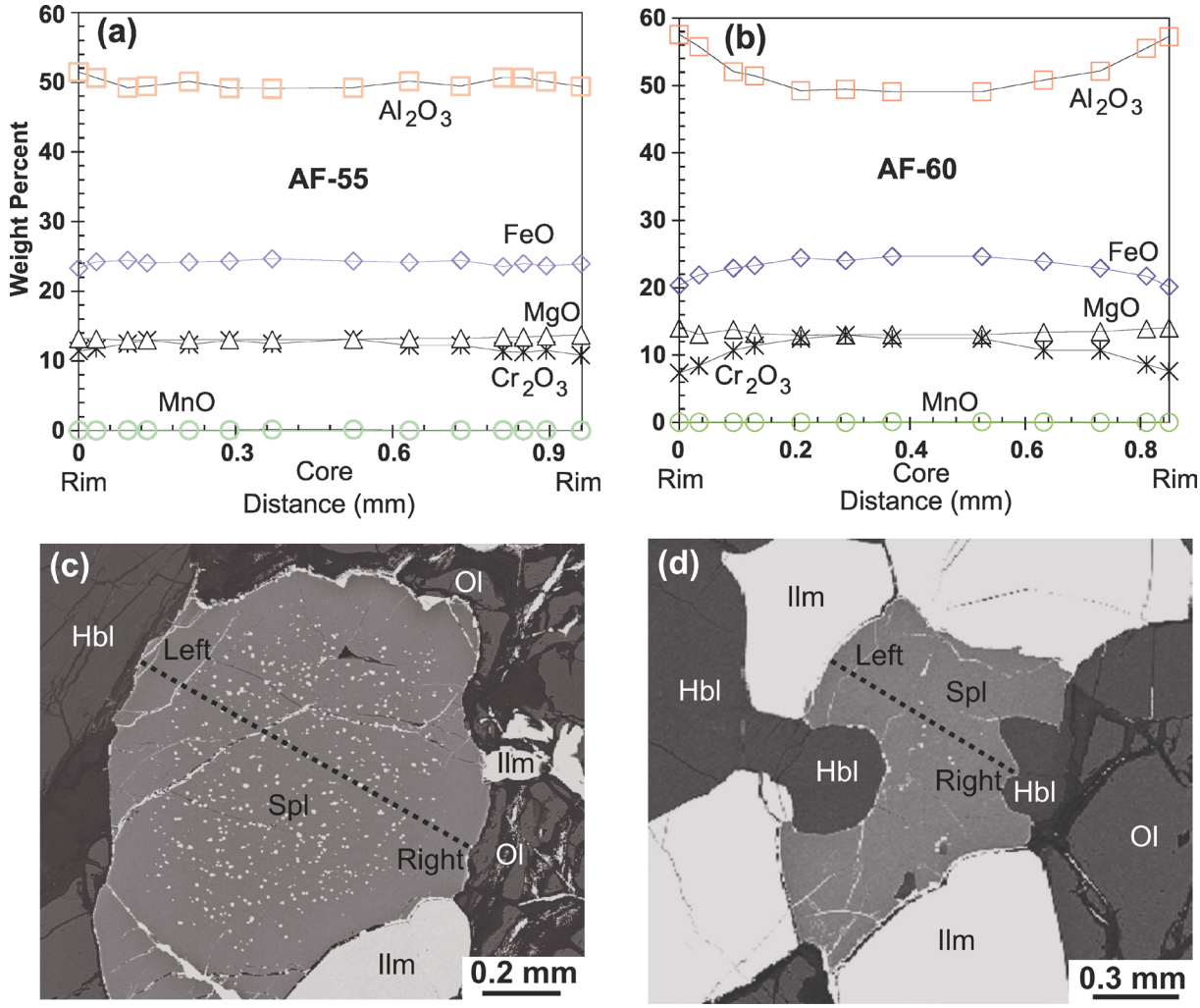

Fig. 5. Compositional variation from rim to rim in spinel crystals and BSE images from some thin sections from high-grade ultramafic schists. **a, b** — Spinel grains from middle to upper amphibolite facies (samples 55 and 60). **c, d** — BSE images from samples 55 and 60 show crosses of analyzed spinel crystals. Abbreviations for minerals are shown in Figure 3.

are the same (Supplementary Table S2). Cln crystals are the cause of preferential orientation and can also occur in some samples with a moderate degree of metamorphism.

Geothermobarometry

We used conventional geothermobarometers, discrimination diagrams, and phase diagram modeling to estimate the metamorphic P–T conditions of the studied rocks.

Conventional thermometers

Temperatures are estimated between 660 and 690 °C for the high-grade mineral assemblages (samples 55 and 60) (Supplementary Table S3) based on the geothermometer equation from Anderson et al. (1972), Bishop (1980) and Sack & Ghiorso (1991). Opx grains, which were in equilibrium with Ol, green Spl, and Ilm, from the high-grade ultramafic rocks of the Qori metamorphic complex, showed temperatures between 640 and 710 °C (Supplementary Table S3) based on the geothermometer equation from Gasparik (1985, 1987). Moreover, the results of the geothermometer of Brey & Köhler (1990)' showed that Opx in the QMC meta-ultramafic rocks formed at 656–756 °C and 5–9 kbar (see the description of Supplementary Table S3).

Discrimination diagrams

The Cr–Fe^{3+}–Al ternary discrimination diagram (Evans & Frost 1975) for Spl grains from rocks formed in different metamorphic grades is illustrated in Fig. 7a. The Spl grains from the studied rocks plot close to the Al apex with the higher-grade metamorphic samples (samples 55 and 60).

At given P, T, and $f_{H2O,}$ the coexistence of spinel and two magnesium silicate minerals sufficed to control the Al_2O_3-content of the chrome-Spl (Fig. 7a). This was by the following equilibria (in order of increasing grade) that existed in these rocks (Evans & Frost 1975):

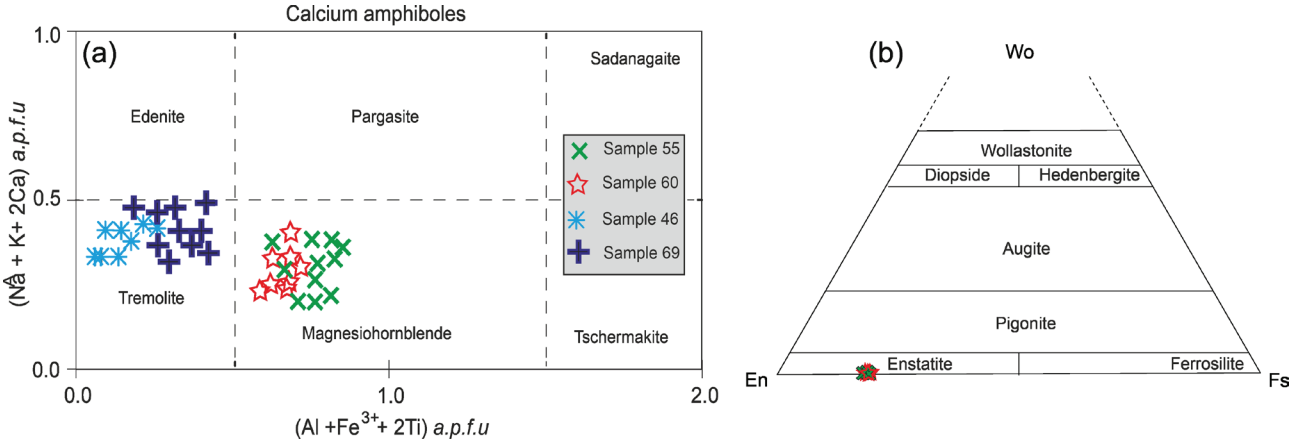

Fig. 6. a — The chemical composition of Amp in various types of ultramafic schists from the QMC. Amp grains vary from Tr and magnesiohornblende in the low-grade to high-grade rocks, respectively. The diagram is from Hawthorne et al. (2012); **b** — Classification of the studied Opx using the En–Wo–Fs ternary diagram (Morimoto et al. 1988).

$$5\ Chl = 2\ Tlc + 7\ Ol + 5\ MgAl_2O_4 + 18\ H_2O$$
$$9\ Chl = 2\ Cum + 11\ Ol + 9\ MgAl_2O_4 + 34\ H_2O$$
$$Chl = 2\ En\ (Opx) + Ol + MgAl_2O_4 + 4\ H_2O$$

In these equations, $MgAl_2O_4$ is the solid solution in the Spl phase, and the formula adapted for chlorite is $Mg_5Al_2Si_3O_{10}(OH)_8$. The latter is a kind of simplification since the Al content in Chl in these parageneses increases with the metamorphic grade. With the constant P and f_{H2O}, the ratio $Al/(Al+Cr+Fe^{3+})$ of Spl in these equilibria could decline with the falling temperature in the manner shown in Figure 8. Spl from the samples 55 and 60 plot on the upper right of the diagram. Fine Spl and Chl grains around the Ol and Opx grains (Fig. 3c, d) are evidence for the above reactions.

Figure 7c shows fields of Chr grains from the layered intrusions and alpine peridotites, as well as different metamorphic facies for ultramafic rocks (modified after Evans & Frost 1975; Hartmann & Chemale-Júnior 2003). Spl minerals from high-grade samples (55 and 60) have low Cr/(Cr+Al) ratios that conformed to amphibolite facies. The calculated curves for the Fe–Mg exchange between Ol and $(Fe, Mg)(Al, Cr)_2O_4$ (Spl; Fig. 7d) as proposed by Sack & Ghiorso (1991) exhibited temperatures between 600 and 700 °C for the samples 55 and 60.

Phase diagram modeling

The calculated pseudosection diagram is represented in Fig. 8a. The diagram shows that the assemblage Ol+Opx+Cpx+Amp+Spl, which was identified as the peak metamorphic assemblage, occurs at 750 to 800 °C and 6 to 8 kbar (field 1). This is consistent with conventional geothermobarometric calculation results (730 and 775 °C and 6.7 and 7.7 kbar).

In T<650 °C, the assemblages contain two Amp crystals ($Amph_1$ and $Amph_2$) that occur with high and low Tr contents respectively, which is in accordance with the Amp compositions of the samples (Fig. 6a). Ol and Spl appear at T>700 °C, and Chl leaves the system. This is consistent with the petrography studies showing that Cln was replaced by Spl and Ol (Fig. 3). To the higher P, the fields contain Grt, which is not present in our samples. Field 2 represents the Amp1+Amp2+Chl+Ol retrograde assemblage in T<650 °C and is identified in the thin sections (Fig. 3). The results are compatible to previous research on phase diagram modeling of the other rocks in the complex (Miri & Fazlnia 2024).

The Al in Opx and Fe/(Fe+Mg) in Ilm isopleths were also calculated to examine the P–T stability of field 1 for the sample (Fig. 8b). The minimum Al (0.06 a.p.f.u) and Fe# (0.8) isopleths intersects at approximately 750 °C and 7 kbar. However, the higher Opx Al contents (0.08 a.p.f.u) indicates that the sample may endure some higher temperatures during peak conditions.

Discussion

Tectonic setting of the area

The geodynamic evolution of the SaSZ has been a controversial topic in the last few years. As mentioned previously, it has traditionally been considered an active continental margin during the Jurassic (Berberian & King 1981; Alavi 1994 Mohajjel & Fergusson 2014; Azizi et al. 2015; Hassanzadeh & Wernicke 2016). A new theory, however, suggests that the Jurassic magmatic activities in the northern part of the SaSZ were not a result of continental rift propagation (Azizi & Stern 2019). Maghdour Mansour et al. (2021) proposed an episodic subduction model where trench retreat was followed by small-scale OIB-like magmatic activity for the Jurassic magmatism of the SaSZ, especially with regards to the dominance of calc-alkaline rocks in all the sectors of the zone. They proposed two stages of orogens, the Early–Middle Jurassic (195–168 Ma) and Middle–Late Jurassic (168–140 Ma), and

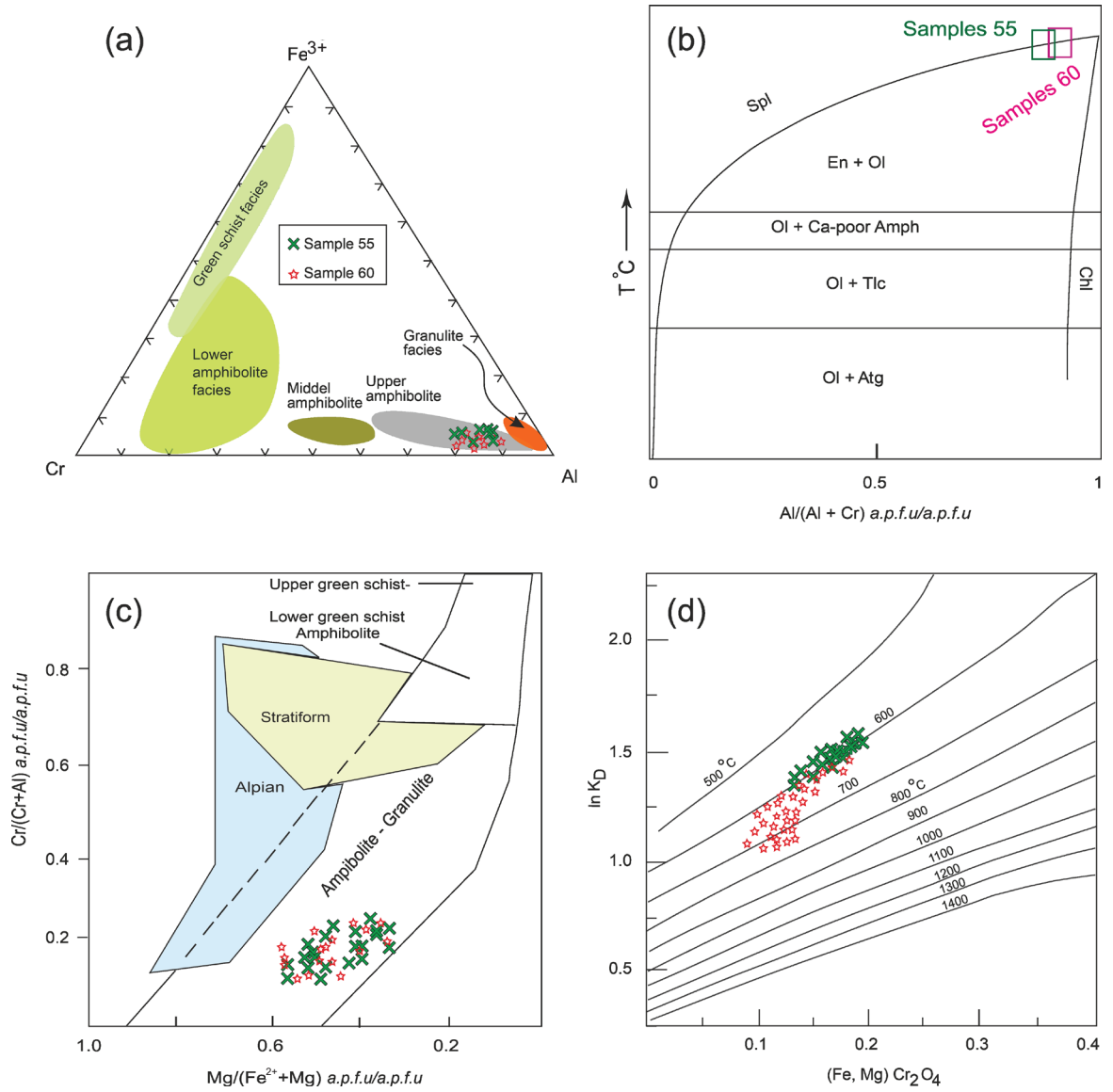

Fig. 7. a — Cr–Al–Fe^{3+} in chrome-Spl of rocks with different metamorphic grades. Data from Evans & Frost (1975) are for comparison; **b** — Schematic phase diagram showing the ratio Al/(Al+Cr) in Spl and Chl (Cln) coexisting with two Mg-silicates and fluid as a function of temperature (after Evans & Frost 1975). The boxes are Al/(Al+Cr) ratios of different samples; **c** — Correlation between 100Cr/(Cr+Al) and XMg for all metamorphic Spl crystals studied. Fields of stratiform and alpine from Evans & Frost (1975); fields of greenschist, amphibolite, and granulite facies from Hartmann & Chemale-Júnior (2003); **d** — Isotherms of ln K_d [$K_d=(X^{Ol}_{Fo}.X^{Spl}_{bulkFe^{2+}})/(X^{Ol}_{Fa}.X^{Spl}_{bulkMg^{2+}})$] for the Fe–Mg exchange between olivine and aluminate-chromite Spl minerals (Sack & Ghiorso 1991). Spl minerals from high-grade metamorphic rocks exhibit different temperatures between 600 and 700 °C.

interpreted the OIB-like magmatism melting of the asthenospheric mantle in response to slab tearing. However, more sedimentology, structural geology, and stratigraphy studies are needed to reconstruct the evolution of the SaSZ Jurassic–Early Cretaceous basin.

So far, no evidence of rifting has been reported in the southern part of the SaSZ during the Jurassic, despite the findings from the central part of this zone by Azizi & Stern (2019) and Nouri et al. (2023). Moreover, magmatism and structural geology studies are not consistent with any continental rift model (Arfania 2018; Yang et al. 2018; Zhang et al. 2018a, b; Gharibnejad et al. 2023; Jafari et al. 2023). In the case of the study area, however, as a part of the south-eastern SaSZ, an active continental margin has been proposed based on geochemical features of the felsic and mafic igneous rocks (e.g., Fazlnia et al. 2007, 2009, 2013; Chiu et al. 2013; Fazlnia 2017b). Yang et al. (2018) considered the gabbroic bodies of the Qory complex as typical continental arc mafic rocks. The Esfandagheh area magmatic rocks (near the study area) also formed on a Jurassic magmatic arc according to Shafaii Moghadam et al. (2017). The Siah-Kuh I-type granitic stock had emplaced at the same time near the study area in

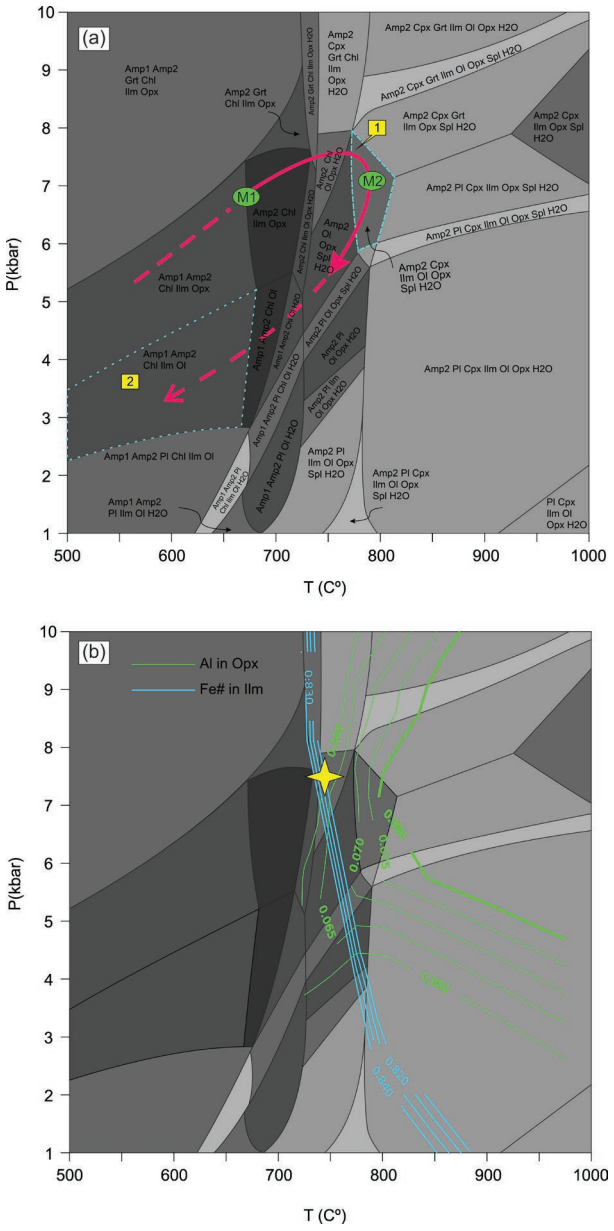

Fig. 8. a — Pseudosection calculated for the sample Af55 in an NCFMASHTO chemical system. **b** — The Al in Opx and Fe/(Fe+Mg) in Ilm isopleths for the calculated pseudosection. The star symbol shows the intersection of the isopleths corresponding to the studied Opx and Ilm (Supplementary Table S2).

association with Neo-Tethys subduction beneath the CIP (Arvin et al. 2007). On the other hand, the Jurassic Barrovian-type medium to high temperature–medium pressure metamorphic events in the area (e.g., Fazlnia et al. 2007, 2009; Sheikholeslami et al. 2008) are not consistent with low-pressure–high-temperature Buchan type metamorphism in the continental rift setting. Therefore, based on all the data, it can be inferred that the area was a part of the NE Neothethys subduction zone during the Jurassic. However, the magmatism was episodic (ca. 170–120 Ma, Fazlnia et al. 2009; Yang et al. 2018).

Metamorphic evolution of the meta-ultramafic rocks

Fazlnia et al. (2007, 2009, 2013) and Fazlnia (2017b) suggested that the Neo-Tethys Ocean expanded until the Late Triassic in the southern part of the SaSZ. By the beginning of the Neo-Tethys lithosphere subduction beneath the CIP at ca. 187–180 Ma (Fazlnia et al. 2007, 2009), crustal thickening and a Barrovian-type metamorphic event (Fig. 9a) occurred. The subduction caused the metasomatization of the mantle wedge above the subduction zone. In the zone of Amp instability and dehydration, other fluids were produced and added to the fluids caused by the dehydration zone of the subduction lithosphere. These fluids migrated to the base of the continental crust and increased the geothermal gradient, resulting in regional metamorphism 187–180 Ma (see Zheng et al. 2016 and Ganne & Feng 2017 for more review). The variation in the slope and subduction angle of the Neo-Tethys (oblique subduction; Jafari et al. 2018, 2022; Balázs et al. 2021) beneath the Central Iran Plate caused partial melting in the mantle wedge (Arfania & Shahriari 2009; Arfania 2018; Jafari et al. 2023); as a consequence, small gabbroic–quartz diorite masses with an age of ~170 Ma (Fazlnia et al. 2013) intruded into the eastern part of the Qori metamorphic complex (Fig. 9b).

Petrographic observations, microprobe analyses, and phase equilibrium modeling together with zircon SHRIMP U–Pb (Fazlnia et al. 2007, 2009) and monazite U–Th-total Pb (CHIME; Fazlnia et al. 2007) ages indicated that the meta-ultramafic rocks from the QMC had a regional metamorphic history involving the medium Barrovian-type metamorphism with a clockwise P–T path. The main metamorphic event in the SaSZ occurred during the early Jurassic in Iran (e.g., Berberian & King 1981), which could be correlated with the final phases of the early Cimmerian orogeny. However, based on the findings of Berberian & Nogol (1974) and Berberian & King (1981), the early Cimmerian orogeny, especially in the CIP, Alburz, and SaSZ, occurred from the Late Triassic to the Late Jurassic. According to Sheikholeslami (2015), the major deformation phase and the major regional metamorphic event took place during the Early Cimmerian orogeny in Late Triassic–Early Jurassic. Late Cimmerian orogeny influenced Iran from the upper Jurassic to the early Cretaceous. Moreover, the study area may have endured a regional metamorphic event related to the Early to Middle Cimmerian orogeny (Fazlnia et al. 2007; Fazlnia 2017b).

The chemical compositions of Spl grains from the QMC high-grade meta-ultrabasic samples, especially in the Seghalaton outcrop (Fig. 1), showed a profile without any change in chemical composition from the core to the nearby rims (flat profile; Fig. 5a–d). The profiles of the cores (e.g., samples 55 and 56) suggest that P–T metamorphic conditions could possibly change after the uniformity of chemical composition due to an increase in metamorphism degree. There were no large and idioblastic grains of Mag in any of the high-grade samples. They occur as accessory phases around Ilm and Spl or as veinlets in Spl (Fig. 4). It is possible that some Mag grains were trapped within Spl and Ilm minerals as a result of

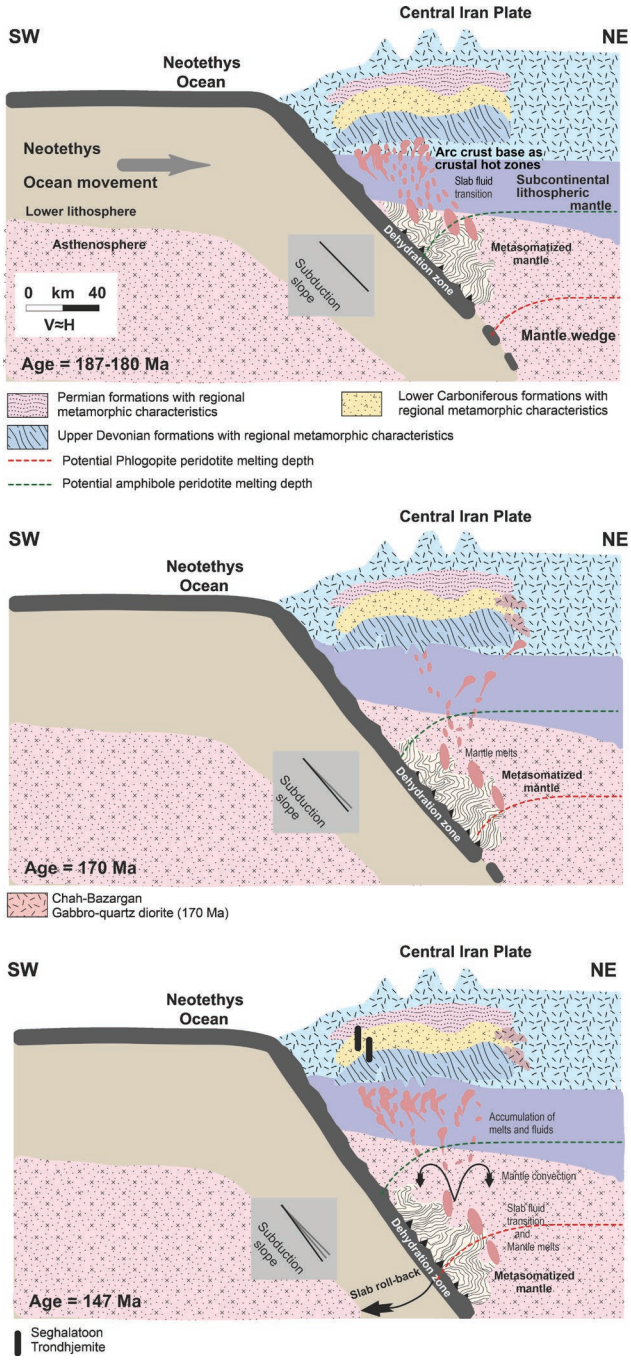

Fig. 9. Tectono-magmatic evolution of the study area located in the southeastern SaSZ. The tectono-magmatic model is drawn based on the data of the new research (Fazlnia et al. 2009; Sheikholeslami 2015; Davoudian et al. 2016; Arfania 2018; Yang et al. 2018; Zhang et al. 2018a, b; Balázs et al. 2021; Stern et al. 2021; Karimpour et al. 2022; Gharibnejad et al. 2023; Jafari et al. 2023). Subduction of the Neo-Tethys oceanic crust beneath the SaSZ (south Eurasia) demonstrates the following results: (a) Evolution of Barrovian-type metamorphism (M1) at ca. 187±2.6 Ma (Fazlnia et al. 2009). The Upper Devonian to Permian formations were metamorphosed during the event. Additionally, at a distance of 150 km away in the south of Qori metamorphic outcrops, Siah Kouh I-type granitic stock (Arvin et al. 2007) was formed. (b) Occurrence of the small mafic–intermediate magmatism such as the Chah-Bazargan gabbro–quartz diorite (170.5±1.9 Ma; Fazlnia et al. 2013). The magmatism was related to the increase in the age and slope of the subduction lithosphere and the increase in the depth of the mantle metasomatism site. (c) Magmatic-fluid activities along transferred heat flow to the SaSZ crust, which resulted in the Neo-Tethys subducted slab beneath the CIP at 147.4±0.76 Ma (Fazlnia et al. 2009), demonstrates the following results: (1) evolution of another Barrovian-type metamorphism (M2) and (2) formation of arc-related trondhjemitic granitic dikes by partial melting of the Grt amphibolite. The depths of the Amp and Phl stability curves from Mandler & Grove (2016) and Safonov et al. (2019), respectively.

the metamorphic prograde reaction. These reactions decreased the modal percentage of Mag and increased the modal percentage of Spl and Ilm. The mutual contact and equilibrium texture for Mag and Ilm likely exhibited the Ilm-Mag buffer for oxygen fugacity during metamorphism.

The ultramafic rocks contained Amp+Cpx+Opx+Cln+Ilm in the M1 P–T condition (Fig. 8a). Variations in the chemical compositions of rims of the Spl grains from the high-grade meta-ultramafic rocks (Fig 5b, d) indicate the occurrence of another metamorphic event. This corresponds to the metamorphic event (M2) at 147.4±0.76 Ma suggested by Fazlnia et al. (2009) and Fazlnia (2017a, b). M2 was associated with the continuation of the subduction of Neo-Tethys beneath the CIP (Fig. 9c) and the heat transfer as a result of the penetration of different types of magmas and the high-temperature fluids from the mantle wedge to the previous metamorphic rocks (M1; 187±2.6 Ma, Fazlnia et al. 2009, 2013; Fig. 9c). The transport of these fluids and melts was intensified by convection in the mantle wedge. The reason for the convective flow in the mantle is the increase in the age of subduction and the thickness of the subducted lithosphere; as a consequence, the rollback of this lithosphere (Zhang et al. 2018a, b; Stern et al. 2021; Karimpour et al. 2022) and the convective flow occur in the mantle wedge (Yang et al. 2018; Balázs et al. 2021; Jafari et al. 2023). These processes caused a high geothermal gradient in the area and caused climax metamorphic conditions in the QMC. The high-grade assemblage Ol+Spl+Opx+Cpx+Amp observed in the studied meta-ultramafic rocks formed due to the M2 event. Moreover, the high geothermal gradient led to partial melting and migmatization of the adjacent Grt amphibolites and the occurrence of trondhjemite veins in the complex reported by Fazlnia et al. (2009) (Fig. 9c). Intrusion of pegmatitic gabbro bodies with Cpx megacrysts in the studied rocks indicates the role of heat transfer and magmatic fluids in metamorphism of the QMC. A similar scenario has been proposed for the regional Barrovian-type metamorphic rocks of the Hamedan area (northern SaSZ) in the Early Jurassic to Early Cretaceous (Sepahi et al. 2019; Saki et al. 2020, 2021; Miri et al. 2024). Our results are consistent with the geodynamic model proposed for the SaSZ with at least two syn-metamorphic regional deformation events together with the intrusion of several igneous bodies during the Jurassic to Early Cretaceous (Cimmerian orogeny; Sheikholeslami 2015; Hassanzadeh & Wernicke 2016; Yang et al. 2018; Jafari et al. 2022, 2023; Karimpour et al. 2022).

Conclusion

Phase relationships and chemistry of minerals (especially Spl) reveal that the QMC meta-ultrabasic rocks formed by at least two Barrovian-type regional metamorphic stages: the first one (M1) at 187±2.6 Ma and the second one (M2) at 147.4±0.76 Ma.

The M1 occurred as a result of crustal thickening and the transfer of mantle wedge fluids during the initiation of the Neo-Tethys subduction beneath the CIP in the Early Jurassic. The M2 was a combined result of increasing the slope of the subduction, intrusion of subduction-associated small magmatic bodies, and fluids accompanied by uplift in the area during the Late Jurassic to Early Cretaceous.

The assemblage Ol+Spl+Opx+Cpx+Amp represents the peak metamorphic condition of the studied rocks formed at 700–800 °C and 6–8 kbar for M2. The retrograde assemblages containing Cln+Tr+Tlc+Atg+Mag formed during exhumation and uplift at T<600 °C and P<5 kbar.

The results of the present study show the role of heat transfer from the subduction zone on the metamorphism of regional metamorphic rocks on the southwestern continental margin of the Iran microplate.

Acknowledgments: The authors would like to thank Volker Schenk, Peter Appel, and Barbara Mader for supporting EMP analyses at Kiel University, Germany. Financial support from the Urmia University (Iran) and Institute für Geowissenschaften, Christian-Albechts-Universität zu Kiel (Germany) is gratefully acknowledged.

References

Agard P., Omrani J., Jolivet L. & Mouthereau F. 2005: Convergence history across Zagros (Iran): constraints from collisional and earlier deformation. *International Journal of Earth Sciences* 94, 401–419. https://doi.org/10.1007/s00531-005-0481-4

Agard P., Omrani J., Jolivet L., Whitechurch H., Vrielynck B., Spakman W., Monie P., Meyer B. & Wortel R. 2011: Zagros orogeny: a subduction-dominated process. *Geological Magazine* 148, 692–725. https://doi.org/10.1017/s001675681100046x

Alavi M. 1994: Tectonic of the Zagros orogenic belt of Iran: new data and interpretations. *Tectonophysics* 229, 211–238. https://doi.org/10.1016/0040-1951(94)90030-2

Anderson A.T., Braziunas T.F., Jacoby J. & Smith J.V. 1972: Thermal and mechanical history of breccias 14306, 14063, 14270, and 14321. In: Proceedings of the Third Lunar Science Conference. *Geochimica et Cosmochimica Acta* 1, 819–835

Arfania R. 2018: Role of supra-subduction zone ophiolites in the tectonic evolution of the southeastern Zagros Orogenic Belt, Iran. *Iran Journal of Earth Science* 10, 31–38.

Arfania R., & Shahriari S. 2009: Role of southeastern Sanandaj–Sirjan Zone in the tectonic evolution of Zagros Orogenic Belt, Iran. *Island Arc* 18, 555–576. https://doi.org/10.1111/j.1440-1738.2009.00680.x

Armstrong J.T. 1995: Citzaf: a package of correction programs for the quantitative electron microbeam X-ray analysis of thick polished materials, thin films and particles. *Microbeam Analysis* 4, 117–200.

Arvin M., Pan Y., Dargahi S., Malekizadeh A. & Babaei A. 2007: Petrochemistry of the Siah-Kuh granitoid stock southwest of Kerman, Iran: Implications for initiation of Neotethys subduction. *Journal of Asian Earth Sciences* 30, 474–489. https://doi.org/10.1016/j.jseaes.2007.01.001

Azizi H. & Stern R.J. 2019: Jurassic igneous rocks of the central Sanandaj–Sirjan zone (Iran: mark a propagating continental rift, not a magmatic arc. *Terra Nova* 31, 415–423. https://doi.org/10.1111/ter.12404

Azizi H., Najari M., Asahara Y., Catlos E..J., Shimizu M. & Yamamoto K. 2015: U–Pb zircon ages and geochemistry of Kangareh and Taghiabad mafic bodies in northern Sanandaj–Sirjan Zone, Iran: evidence for intra-oceanic arc and back-arc tectonic regime in Late Jurassic. *Tectonophysics* 660, 47–64. https://doi.org/10.1016/j.tecto.2015.08.008

Balázs A., Faccenna C., Ueda K., Funiciello F., Boutoux A., Blancd E.J.P. & Gerya T. 2021: Oblique subduction and mantle flow control on upper plate deformation: 3D geodynamic modeling. *Earth and Planetary Science Letters* 569, 117056. https://doi.org/10.1016/j.epsl.2021.117056

Berberian F. & Berberian M. 1981: Tectono-plutonic episodes in Iran. *American Geophysical Union, Geodynamics series* 3, 5–32. https://doi.org/10.1029/GD003p0005

Berberian M. & King G.C.P. 1981: Towards a paleogeography and tectonic evolution of Iran. *Canadian Journal of Earth Science* 18, 210–265. https://doi.org/10.1139/e81-019

Berberian M. & Nogol M. 1974: Preliminary explanatory text of the geology of Deh Sard and Khabr maps with some remarks on the metamorphic complexes and the tectonics of the area (two geological maps, 1:100,000, from the Hajjiabad quadrangle map). *Geological survey of Iran, internal report*, 1–60.

Bishop F.C. 1980: The distribution of Fe^{2+} and Mg between coexisting ilmenite and pyroxene with applications to geothermometry. *American Journal of Science* 280, 46–77. https://doi.org/10.2475/ajs.280.1.46

Brey G.P. & Köhler T. 1990: Geothermobarometry in four-phase lherzolites II. New thermobarometers, and practical assessment of existing thermobarometers. *Journal of Petrology* 31, 1353–1378. https://doi.org/10.1093/petrology/31.6.1353

Chiu H.-Y., Chung S.-L., Zarrinkoub M.H., Mohammadi S.S., Khatib M.M. & Iizuka Y. 2013: Zircon U–Pb age constraints from Iran on the magmatic evolution related to Neotethyan subduction and Zagros orogeny. *Lithos* 162, 70–87. https://doi.org/10.1016/j.lithos.2013.01.006

Connolly J.A. 2005: Computation of phase equilibria by linear programming: a tool for geodynamic modeling and its application to subduction zone decarbonation. *Earth and Planetary Science Letters* 236, 524–541. https://doi.org/10.1016/j.epsl.2005.04.033

Davoudian A.R., Gense G., Neubauer F. & Shabanian N. 2016: $^{40}Ar/^{39}Ar$ mineral ages of eclogites from North Shahrekord in the Sanandaj–Sirjan Zone, Iran: Implications for the tectonic evolution of Zagros orogeny. *Gondwana Research* 37, 216–240. https://doi.org/10.1016/j.gr.2016.05.013

Dilek Y., Imamverdiyev N. & Altunkaynak S. 2010: Geochemistry and tectonics of Cenozoic volcanism in the Lesser Caucasus (Azerbaijan) and the peri-Arabian region: collision-induced mantle dynamics and its magmatic fingerprint. *International Geology Review* 52, 536–578. https://doi.org/10.1080/00206810903360422

Evans B.W. & Frost B.R. 1975: Chrome-spinel in progressive metamorphism: A preliminary analysis. *Geochim Cosmochim Acta* 39, 959–972. https://doi.org/10.1016/b978-0-08-019954-2.50020-2

Eyuboglu Y., Santosh M., Yi K., Bektaş O. & Kwon S. 2012: Discovery of Miocene adakitic dacite from the Eastern Pontides Belt and revised geodynamic model for the late Cenozoic Evolution

of eastern Mediterranean region. *Lithos* 146–147, 218–232. https://doi.org/10.1016/j.lithos.2012.04.034

Fazlnia A.N. 2017a: The evolution of arc magmatism related to Palaeotethys in the west of Salmas, north of the Sanandaj–Sirjan Zone, Iran. *Geological Quarterly* 61, 124–137. https://doi.org/10.7306/gq.1339

Fazlnia A.N. 2017b: Geochemical characteristics and conditions of formation of the Chah-Bazargan peraluminous granitic patches, ShahrBabak, Iran. *Geolgica Carpathica* 68, 445–463. https://doi.org/10.1515/geoca-2017-0029

Fazlnia A.N. 2018: Geochemistry and tectonic setting of the Chah-Bazargan sub-volcanic mafic dykes, south Sanandaj–Sirjan Zone (SaSZ), Iran. *Geological Quarterly* 62, 447–458. https://doi.org/10.7306/gq.1417

Fazlnia A.N. 2019: Petrogenesis and tectonic significance of Sardasht syenite–monzonite–gabbro–appinite intrusions, NW Iran. *International Journal of Earth Sciences* 108, 49–66. https://doi.org/10.1007/s00531-018-1641-7

Fazlnia AN. & Alizade A. 2013: Petrology and geochemistry of the Mamakan gabbroic intrusions, Urumieh (Urmia), Iran: Magmatic development of an intra-oceanic arc. *Periodico di Mineralogia* 82, 263–290.

Fazlnia A.N., Moradian A., Rezaei K., Moazzen M. & Alipour S. 2007: Synchronous Activity of Anorthositic and S-type Granitic magmas in Chah-Dozdan batholith, Neyriz, Iran: Evidence of Zircon SHRIMP and Monazite CHIME Dating. *Iran Journal of Science* 18, 221–237. https://doi.org/10.1007/s00410-018-1520-z

Fazlnia A.N, Schenk V., van der Straaten F. & Mirmohammadi M. 2009: Petrology, Geochemistry, and Geochronology of Trondhjemites from the Qori Complex, Neyriz, Iran. *Lithos* 112, 413–433. https://doi.org/10.1016/j.lithos.2009.03.047

Fazlnia A.N., Schenk V., Appel P. & Alizade A. 2013: Petrology, geochemistry, and geochronology of the Chah-Bazargan gabbroic intrusions in the south Sanandaj–Sirjan zone, Neyriz, Iran. *International Journal of Earth Sciences* 102, 1403–1426. https://doi.org/10.1007/s00531-013-0884-6

Fergusson C.L., Nutman A.P., Mohajjel M. & Bennett V.C. 2016: The Sanandaj–Sirjan Zone in the Neo-Tethyan suture, western Iran: Zircon U–Pb evidence of late Palaeozoic rifting of northern Gondwana and mid-Jurassic orogenesis. *Gondwana Research* 40, 43–57. https://doi.org/10.1016/j.gr.2016.08.006

Fusheng G., Guo S., Qingkun Y., Wanliang Z., Caifu X., Wanpeng Z. & Jiewei Z. 2018: Timing of Metamorphism and Provenance of the Metamorphic Basement of the Xiangshan Uranium Orefield, Jiangxi Province, China. *Acta Geologica Sinica* 92, 34–55. https://doi.org/10.1111/1755-6724.13493

Ganne J. & Feng X. 2017: Primary magmas and mantle temperatures through time. *Geochemistry Geophysics Geosystems* 18, 872–888. https://doi.org/10.1002/2016gc006787

Gasparik T. 1985: The orthopyroxene–clinopyroxene–olivine–spinel geothermometer in the system CaO–FeO–MgO–Al_2O_3–SiO_2 (CFMAS). The 23rd General Assembly of IASPEI abstracts, Tokyo, 1–312.

Gasparik T. 1987: Orthopyroxene thermobarometry in spinel and complex system. *Contribution to Mineralogy and Petrology* 96, 357–370. https://doi.org/10.1007/bf00371254

Gharibnejad P., Rosenberg C.L., Agard P., Kananian K. & Omrani J. 2023: Structural and metamorphic evolution of the southern Sanandaj-Sirjan zone, southern Iran. *International Journal of Earth Sciences* 112, 383–415. https://doi.org/10.1007/s00531-022-02255-5

Golonka J. 2004: Plate tectonic evolution of the southern margin of Eurasia in the Mesozoic and Cenozoic. *Tectonophysics* 381, 235–273. https://doi.org/10.1016/j.tecto.2002.06.004

Green D.H. 2015: Experimental petrology of peridotites, including effects of water and carbon on melting in the Earth's upper mantle. *Physics and Chemistry of Minerals* 42, 95–122. https://doi.org/10.1007/s00269-014-0729-2

Green E., White R., Diener J., Powell R., Holland T., & Palin R. 2016: Activity–composition relations for the calculation of partial melting equilibria in metabasic rocks. *Journal of Metamorphic Geology* 34, 845–869. https://doi.org/10.1111/jmg.12211

Hartmann L.A. & Chemale-Júnior F. 2003: Mid amphibolite facies metamorphism of harzburgites in the Neoproterozoic Cerro Manttiqueiras ophiolite, southernmost Brazil. *Anais da Academia Brasileira de Ciências* 75, 109–128. https://doi.org/10.1590/s0001-37652003000100012

Hassanzadeh J. & Wernicke BP. 2016: The Neotethyan Sanandaj–Sirjan zone of Iran as an archetype for passive margin-arc transitions. *Tectonics* 35, 586–621. https://doi.org/10.1002/2015tc003926

Hawthorne F.C., Oberti R., Harlow G.E., Maresch W.V., Martin R.F., Schumacher J.C. & Welch M.D. 2012: Nomenclature of the amphibole supergroup. *American Mineralogist* 97, 2031–2048. https://doi.org/10.2138/am.2012.4276

Holland T. & Powell R. 2003: Activity-compositions relations for phases in petrological calculations: An asymetric multicomponent formulation. *Contributions to Mineralogy and Petrology* 145, 492–501. https://doi.org/10.1007/s00410-003-0464-z

Holland T.J.B. & Powell R. 1998: An internally consistent thermodynamic data set for phases of petrological interest. *Journal of Metamorphic Geology* 16, 309–43. https://doi.org/10.1111/j.1525-1314.1998.00140.x

Holland T.J.B. & Powell R. 2011. An improved and extended internally consistent thermodynamic dataset for phases of petrological interest, involving a new equation of state for solids. Journal of Metamorphic Geology 29, 333–383. https://doi.org/10.1111/j.1525-1314.2010.00923.x

Honarmand M., Li X., Nabatian G. & Neubauer F. 2017: In-situ zircon U–Pb age and Hf-Oisotopic constraints on the origin of the Hasan-Robat A-type granite from Sanandaj–Sirjan zone, Iran: implications for reworking of Cadomian arc igneous rocks. *Mineralogy and Petrology* 111, 659–675. https://doi.org/10.1007/s00710-016-0490-y

Jafari A., Fazlnia A.N. & Jamei S. 2015: Mafic enclaves in north of Urumieh plutonic complex: evidence of magma mixing and mingling, Sanandaj–Sirjan zone, NW Iran. *Arabian Journal of Geoscience* 8, 7191–7206. https://doi.org/10.1007/s12517-014-1701-7

Jafari A., Fazlnia A.N. & Jamei S. 2018: Geochemistry, petrology and geodynamic setting of the Urumieh plutonic complex, Sanandaj–Sirjan zone, NW Iran: new implication for Arabian and Central Iranian plate collision. *Journal of African Earth Science* 139, 421–439. https://doi.org/10.1016/j.jafrearsci.2017.11.039

Jafari A., Williams I.S., Moayyed M. & Jamei S. 2022: Physical and chemical interactions between coeval magmas: a case study of mixing and mingling from the Urumieh plutonic complex, NW Iran. *International Geology Review* 64, 489–508. https://doi.org/10.1080/00206814.2020.1858454

Jafari A., Ao S., Jamei S. & Ghasemi H. 2023: Evolution of the Zagros sector of Neo-Tethys: Tectonic and magmatic events that shaped its rifting, seafloor spreading and subduction history. *Earth Science Reviews* 241, 104419. https://doi.org/10.1016/j.earscirev.2023.104419

Karimi S., Tabatabaei Manesh S.M., Safaei H. & Sharifi M. 2012: Metamorphism and Deformation of Golpayegan Metapelitic Rocks, Sanandaj–Sirjan Zone, Iran. *Petrology* 20, 658–675. https://doi.org/10.1134/s086959111207003x

Karimpour M.H., Shirdashtzadeh N. & Sadeghi M. 2022: Tectonomagmatic settings of Jurassic granitoids in the Sanandaj–Sirjan Zone, Iran: A review. *Geologos* 28, 19–37. https://doi.org/10.2478/logos-2022-0002

Khadivi S., Mouthereau F., Barbarand J., Adatte T. & Lacombe O. 2012: Constraints on paleodrainage evolution induced by uplift and exhumation on the southern flank of the Zagros–Iranian Plateau. *Journal of Geological Society* 169, 83–97. https://doi.org/10.1144/0016-76492011-031

Lucci F., Saki A., Miri M., Rabiee A. & White J.C. 2021: Genesis of trondhjemite by low-pressure low-melt fraction anatexis of hornblende-gabbro at Alvand Plutonic Complex (Hamedan, NW Iran): insights from geochemical modelling. *Arabian Journal of Geosciences*, 14, 1–20. https://doi.org/10.1007/s12517-021-08104-0

Lucci F., Miri M., Saki A., White J.C., Della Ventura G. & Azizi H. 2023: The Middle Jurassic Cheshmeh-Ghasaban High-Mg gabbro (Hamedan, NW Iran): A plume-influenced intracontinental rifting event?. *Geochemistry* 83, 126011. https://doi.org/10.1016/j.chemer.2023.126011

Maghdour-Mashhour R., Hayes B., Pang K.N., Bolhar R., Shabani A.A.T. & Elahi-Janatmakan F. 2021: Episodic subduction initiation triggered Jurassic magmatism in the Sanandaj–Sirjan zone, Iran. *Lithos* 396, 106189. https://doi.org/10.1016/j.lithos.2021.106189

Mahmoudi S. & Baharifar A.A. 2018: Phase equilibria and P–T–t path of metapelitic rocks in SE-Hamedan, Sanandaj–Sirjan Zone, Iran. *Mineralogy and Petrology* 113, 135–154. https://doi.org/10.1007/s00710-018-0635-2

Mandler B.E. & Grove T.L. 2016: Controls on the stability and composition of amphibole in the Earth's mantle. *Contributions to Mineralogy and Petrology* 171, 68. https://doi.org/10.1007/s00410-016-1281-5

Miri M. & Fazlnia A. 2024: Investigating the progressive dynamothermal metamorphic evolution of metabasites from the Qori complex (NE Neyriz) using phase diagrams. *Advanced Applied Geology* 13, 1176–1192. https://doi.org/10.22055/AAG.2024.44786.2403

Miri M. & Sepahi A.A. 2023: High-pressure–Low-temperature metamorphic rocks of Iran and their geodynamic significance: A review. *Journal of Geodynamics* 157, 101986. https://doi.org/10.1016/j.jog.2023.101986

Miri M., Sepahi A.A., Maanijou M. & Lucci F. 2024: Rare earth element (REE) partitioning in amphibole-bearing medium grade metamorphic rocks from the Alvand Complex (Sanandaj–Sirjan Zone, NW Iran). *Periodico di Mineralogia* 93, 11–33. https://doi.org/0.13133/2239-1002/18284

Mohajjel M. & Fergusson C.L. 2014: Jurassic to Cenozoic tectonics of the Zagros Orogen in northwestern Iran. *International Geology Review* 56, 263–287. https://doi.org/10.1080/00206814.2013.853919

Moinvaziri H., Akbarpour A. & Azizi H. 2015: Mesozoic magmatism in the northwestern Sanandaj–Sirjan zone as an evidence for active continental margin. *Arabian Journal of Geoscience* 8, 3077–3088. https://doi.org/10.1007/s12517-014-1309-y

Molinaro M., Zeyen H. & Laurencin X. 2005: Lithospheric structure beneath the south-eastern Zagros Mountains, Iran recent slab break-Mountains, Iran recent slab break-off. *Terra Nova* 17, 1–6. https://doi.org/10.1111/j.1365-3121.2004.00575.x

Morimoto N., Fabrise J., Ferguson A., Ginzburg I.V., Ross M., Seifert F.A. & Gottardi G. 1988: Nomenclature of pyroxenes. *American Mineralogist* 173, 1123–1133. https://doi.org/10.3406/bulmi.1988.8099

Mouthereau F., Lacombe O. & Vergés J. 2012: Building the Zagros collisional orogen: Timing, strain distribution and the dynamics of Arabia/Eurasia plate convergence. *Tectonophysics* 532–535, 27–60. https://doi.org/10.1016/j.tecto.2012.01.022

Nadimi A. 2015: Structural Analysis of the Hasan_Robat Marbles as Traces of Folded Basement in the Sanandaj–Sirjan Zone, Iran. *Geotectonics* 49, 560–578. https://doi.org/10.1134/s0016852115060060

Neill I., Meliksetian K., Allen M.B., Navasardyan G. & Karapetyan S. 2013: Pliocene–Quaternary volcanic rocks of NW Armenia: Magmatism and lithospheric dynamics within an active orogenic plateau. *Lithos* 180–181, 200–215. https://doi.org/10.1016/j.lithos.2013.05.005

Neill I., Meliksetian K., Allen M.B., Navasardyan G. & Kuiper K. 2015: Petrogenesis of mafic collision zone magmatism: The Armenian sector of the Turkish–Iranian Plateau. *Chemical Geology* 403, 24–41. https://doi.org/10.1016/j.chemgeo.2015.03.013

Nouri F., Azizi H., Stern R. & Asahara Y. 2023: The Sanandaj–Sirjan Zone (W. Iran: was a Jurassic passive continental margin: Evidence from igneous rocks of the Songhor area. *Lithos* 440–441, 107023. https://doi.org/10.1016/j.lithos.2023.107023

Omrani J., Agard P., Whitechurch H., Benoit M., Prouteau G. & Jolivet L. 2008: Arc magmatism and subduction history beneath the Zagros Mountains, Iran: a new report of adakites and geodynamic consequences. *Lithos* 106, 380–398. https://doi.org/10.1016/j.lithos.2008.09.008

Peltonen P. 1990: Metamorphic olivine in picritic metavolcanics from southern Finland. *Bulletin of Geology Society of Finland* 62, 99–114. https://doi.org/10.17741/bgsf/62.2.001

Sabzehei M., Navazi M., Ghavidel M. & Hamdi S.B. 1992: Geological map of Neyriz (1/250,000). *Geological Survey of Iran*.

Sack O.S. & Ghiorso M.S. 1991: Chromian spinels as petrogenetic indicators: Thermodynamics and petrological applications. *American Mineralogist* 76, 827–847.

Safonov O., Butvina V. & Limanov E. 2019: Phlogopite-Forming Reactions as Indicators of Metasomatism in the Lithospheric Mantle. *Minerals* 9, 685. https://doi.org/10.3390/min9110685

Saki A., Miri M. & Oberhansli R. 2020: High temperature–low pressure metamorphism during subduction of Neo-Tethys beneath the Iranian plate: evidence for mafic migmatite formation in the Alvand complex (western Iran). *Mineralogy and Petrology* 114, 539–557. https://doi.org/10.1007/s00710-020-00721-z

Saki A., Lucci F, Miri M. & White J. 2021: Trondhjemite leucosomes generated by partial melting of a hornblende-gabbro (Alvand plutonic complex, Hamedan, NW Iran). *International Geology Review* 64, 597–630. https://doi.org/10.1080/00206814.2020.1861554

Sepahi A.A., Shahbazi H., Siebel W. & Ranin A. 2014: Geochronology of plutonic rocks from the Sanandaj–Sirjan zone, Iran and new zircon and titanite U–Th–Pb ages for granitoids from the Marivan pluton. *Geochronometria* 41, 207–215. https://doi.org/10.2478/s13386-013-0156-z

Sepahi A.A, Jafari S.R., Osanai Y., Shahbazi H. & Moazzen M. 2019: Age, petrologic significance and provenance analysis of the Hamedan low-pressure migmatites; Sanandaj-Sirjan zone, West Iran. *International Geology Review* 61, 1446–1461. https://doi.org/10.1080/00206814.2018.1517392

Shabanian N., Davoudian A.R., Dong Y. & Liu X. 2018: U–Pb zircon dating, geochemistry and Sr–Nd–Pb isotopic ratios from Azna–Dorud Cadomian metagranites, Sanandaj–Sirjan Zone of Western Iran. *Precambrian Research* 306, 41–60. https://doi.org/10.1016/j.precamres.2017.12.037

Shafaii Moghadam H., Ghorbani G., Zaki Khedr M., Fazlnia A.N., Chiaradia M., Eyuboglu Y., Santosh M., Galindo Francisco C., Lopez Martinez M., Gourgaud A. & Arai S. 2014: Late Miocene K-rich volcanism in the Eslamieh Peninsula (Saray), NW Iran: Implications for geodynamic evolution of the Turkish–Iranian High Plateau. *Gondwana Research* 26, 1028–1050. https://doi.org/10.1016/j.gr.2013.09.015

Shafaii Moghadam H., Li X-H., Stern R.J., Ghorbani G. & Bakhshizad F. 2016: Zircon U–Pb ages and Hf–O isotopic composition of migmatites from the Zanjan–Takab complex, NW Iran: Constraints on partial melting of metasediments. *Lithos* 240–243, 34–48. https://doi.org/10.1016/j.lithos.2015.11.004

Shafaii Moghadam H., Bröcker M., Griffin W.L., Li X.H., Chen R.X. & O'Reilly S.Y. 2017: Subduction, high-P metamorphism, and collision fingerprints in South Iran: Constraints from zircon U–Pb and mica Rb–Sr geochronology. *Geochemistry, Geophysics, Geosystems* 18, 306–332. https://doi.org/10.1002/2016GC006585

Sheikholeslami MR. 2015: Deformations of Palaeozoic and Mesozoic rocks in southern Sirjan, Sanandaj–Sirjan Zone, Iran. *Journal of Asian Earth Science* 106, 130–149. https://doi.org/10.1016/j.jseaes.2015.03.007

Sheikholeslami M.R., Pique A., Mobayen P., Sabzehei M., Bellon H. & Emami M.H. 2008: Tectono-metamorphic evolution of the Neyriz metamorphic complex, Quri-Kor-e-Sefid area (Sanandaj-Sirjan Zone, SW Iran). *Journal of Asian Earth Science* 31, 504–521. https://doi.org/10.1016/j.jseaes.2007.07.004

Stern R.J., Shafaii Moghadam H., Pirouz M. & Mooney W. 2021: The Geodynamic Evolution of Iran. *Annual Review in Earth and Planetary Sciences* 49, 9–36. https://doi.org/10.1146/annurev-earth-071620-052109

Stöcklin J. 1968: Structural history and tectonics of Iran: a review. AAPG Bulletin 52, 1229–1258.

White R., Powell R. & Clarke G. 2002: The interpretation of reaction textures in Fe-rich metapelitic granulites of the Musgrave Block, central Australia: constraints from mineral equilibria calculations in the system K_2O–FeO–MgO–Al_2O_3–SiO_2–H_2O–TiO_2–Fe_2O_3. *Journal of Metamorphic Geology* 20, 41–55. https://doi.org/10.1046/j.0263-4929.2001.00349.x

White R.W., Powell R., Holland T.J.B. & Worley B.A. 2000: The effect of TiO_2 and Fe_2O_3 on metapelitic assemblages at greenschist and amphibolite facies conditions: mineral equilibria calculations in the system K_2O–FeO–MgO–Al_2O_3–SiO_2–H_2O–TiO_2–Fe_2O_3. *Journal of Metamorphic Geology* 18, 497–511. https://doi.org/10.1046/j.1525-1314.2000.00269.x

White R.W., Powell R., Holland T., Johnson T. & Green E. 2014: New mineral activity–composition relations for thermodynamic calculations in metapelitic systems. *Journal of Metamorphic Geology* 32, 261–286. https://doi.org/10.1111/jmg.12071

Whitney D.L. & Evans B.W. 2010: Abbreviations for names of rock-forming minerals. *American Mineralogist* 95, 185–187. https://doi.org/10.2138/am.2010.3371

Yang T.N., Chen J.L., Liang M.J., Xin D., Aghazadeh M., Hou Z.Q. & Zhang H. 2018: Two plutonic complexes of the Sanandaj–Sirjan magmatic–metamorphic belt record Jurassic to Early Cretaceous subduction of an old Neotethys beneath the Iran microplate. *Gondwana Research* 62, 246–268. https://doi.org/10.1016/j.gr.2018.03.016

Zhang H., Chen J., Yang T., Hou Z. & Aghazadeh M. 2018a: Jurassic granitoids in the northwestern Sanandaj–Sirjan Zone: Evolving magmatism in response to the development of a Neo-Tethyan slab window. *Gondwana Research* 62, 269–286. https://doi.org/10.1016/j.gr.2018.01.012

Zhang Z., Xiao W., Ji W., Majidifard M.R., Rezaeian M., Talebia M., Xiang D., Chen L., Wan B., Ao S. & Esmaeili R. 2018b: Geochemistry, zircon U–Pb and Hf isotope for granitoids, NW Sanandaj–Sirjan zone, Iran: Implications for Mesozoic–Cenozoic episodic magmatism during Neo-Tethyan lithospheric subduction. *Gondwana Research* 62, 227–245. https://doi.org/10.1016/j.gr.2018.04.002

Zheng Y.F., Chen R.X., Xu Z. & Zhang S.B. 2016: The transport of water in subduction zones. *Science China Earth Science* 59, 651–682. https://doi.org/10.1007/s11430-015-5258-4

Electronic supplementary material is available online:

Supplementary Table S1 at http://geologicacarpathica.com/data/files/supplements/GC-75-4-Fazlnia_TableS1.xlsx
Supplementary Table S2 at http://geologicacarpathica.com/data/files/supplements/GC-75-4-Fazlnia_TableS2.xlsx
Supplementary Table S3 at http://geologicacarpathica.com/data/files/supplements/GC-75-4-Fazlnia_TableS3.xlsx
Supplementary Table S4 at http://geologicacarpathica.com/data/files/supplements/GC-75-4-Fazlnia_TableS4.xlsx
Supplementary Table S5 at http://geologicacarpathica.com/data/files/supplements/GC-75-4-Fazlnia_TableS5.docx